ARTICLES
PUBLISHED ONLINE: 23 JUNE 2013 | DOI: 10.1038/NPHYS2661
nature physics

Population distribution of product states following three-body recombination in an ultracold atomic gas

A. Härter[1], A. Krükow[1], M. Deiß[1], B. Drews[1], E. Tiemann[2] and J. Hecker Denschlag[1]*

Three-body recombination is a collision process where two atoms combine to form a molecule and a third atom carries away part of the released reaction energy. Here, we experimentally determine for the first time the population distribution of the molecular reaction products after a three-body recombination for non-resonant particle interactions. The key to our measurements is a sensitive detection scheme that combines the photoionization of the molecules with subsequent ion trapping. Using an ultracold ^{87}Rb gas at very low kinetic energy below $h \times 20$ kHz, we find a broad population of final states with binding energies of up to $h \times 750$ GHz. This is in contrast with previous experiments, performed in the resonant interaction regime, that found a dominant population of only the most weakly bound molecular state or the occurrence of Efimov resonances. This work may contribute to the development of an in-depth model that can qualitatively and quantitatively predict the reaction products of three-body recombination.

Whereas cold collisions of two atoms are well understood, the addition of a third collision partner markedly complicates the interaction dynamics. In the context of Bose–Einstein condensation in atomic gases, three-body recombination plays a crucial role[1–4] and it constitutes a present frontier of few-body physics[5–7]. Until now, recombination events were mainly investigated by measuring atom loss rates. Discussions of the final states populated in the recombination process were restricted to the special case of resonant interactions[8,9] and culminated in the observations of Efimov resonances[10–12] and of molecules in the most weakly bound states[13,14]. However, in the more general case of non-resonant interaction, that is, a modulus of the scattering length smaller than or comparable to the van der Waals radius, the recombination products might depend on details of the interaction potential. In fact, ongoing theoretical studies using simplified models indicate that recombination does not necessarily always favour the most weakly bound state (J. d'Incao, private communication; see also ref. 15). In general, recombination processes are of fundamental interest in various physical systems[1,16,17]. The control and tunability of ultracold atomic systems provide an experimental testbed for a detailed understanding of the nature of these processes.

Here, we demonstrate the probing of molecules with binding energies up to $h \times 750$ GHz (where h is Planck's constant) generated through three-body recombination of ultracold thermal ^{87}Rb atoms. We produce the atomic sample in an optical dipole trap located within a linear Paul trap. The recombination and detection process is illustrated in Fig. 1a–d. Following a recombination event, the created Rb_2 molecule can undergo resonance-enhanced multi-photon ionization (REMPI) by absorbing photons from the dipole trap laser at a wavelength of around 1,064.5 nm. The ion is then captured in the Paul trap and detected essentially background-free with very high sensitivity on the single-particle level. Figure 1e shows a simplified scheme of the Rb_2 and Rb_2^+ potential energy curves. From weakly bound molecular states, three photons suffice to reach the molecular ionization threshold. An additional photon may dissociate the molecular ion. By scanning the frequency of the dipole trap laser by more than 60 GHz we obtained a high-resolution spectrum featuring more than 100 resonance peaks. This dense and complex spectrum contains information concerning which vibrational, rotational and hyperfine levels of the Rb_2 molecule are populated. We present an analysis of these data and make a first assignment of the most prominent resonances. This assignment indicates that in the recombination events a broad range of levels is populated in terms of vibrational, rotational, electronic and nuclear spin quantum numbers.

Our experimental scheme to detect cold molecules makes use of the generally excellent detection efficiencies attainable for trapped ions. It is related to proven techniques where cold molecules in magneto-optical traps were photoionized from the singlet and triplet ground states[18–23] (see also ref. 24). Our method is unique as it introduces the use of a hybrid atom–ion trap that significantly improves the detection sensitivity. We perform the following experimental sequence. A thermal atomic sample typically containing $N_{at} \approx 5 \times 10^5$ spin-polarized ^{87}Rb atoms in the $|F = 1, m_F = -1\rangle$ hyperfine state is prepared in a crossed optical dipole trap at a magnetic field of about 5 G. The trap is positioned onto the nodal line of the radiofrequency field of a linear Paul trap. Along the axis of the Paul trap the centres of the atom and ion trap are separated by about 300 μm to avoid unwanted atom–ion collisions (Fig. 1d). At atomic temperatures of about 700 nK and peak densities $n_0 \approx 5 \times 10^{13}$ cm^{-3} the total three-body recombination rate in the gas is $\Gamma_{rec} = L_3 n_0^2 N_{at}/3^{5/2} \approx 10$ kHz. Here, the three-body loss rate coefficient L_3 was taken from ref. 3. At the rate Γ_{rec}, pairs of Rb_2 molecules and Rb atoms are formed as final products of the reactions. Both the atom and molecule would generally be lost from the shallow neutral particle trap owing to the comparatively large kinetic energy they gain in the recombination event (in our case typically of the order of a few $K \times k_B$, where

[1]Institut für Quantenmaterie and Center for Integrated Quantum Science and Technology IQST, Universität Ulm, 89069 Ulm, Germany, [2]Institut für Quantenoptik, Leibniz Universität Hannover, 30167 Hannover, Germany. *e-mail: johannes.denschlag@uni-ulm.de

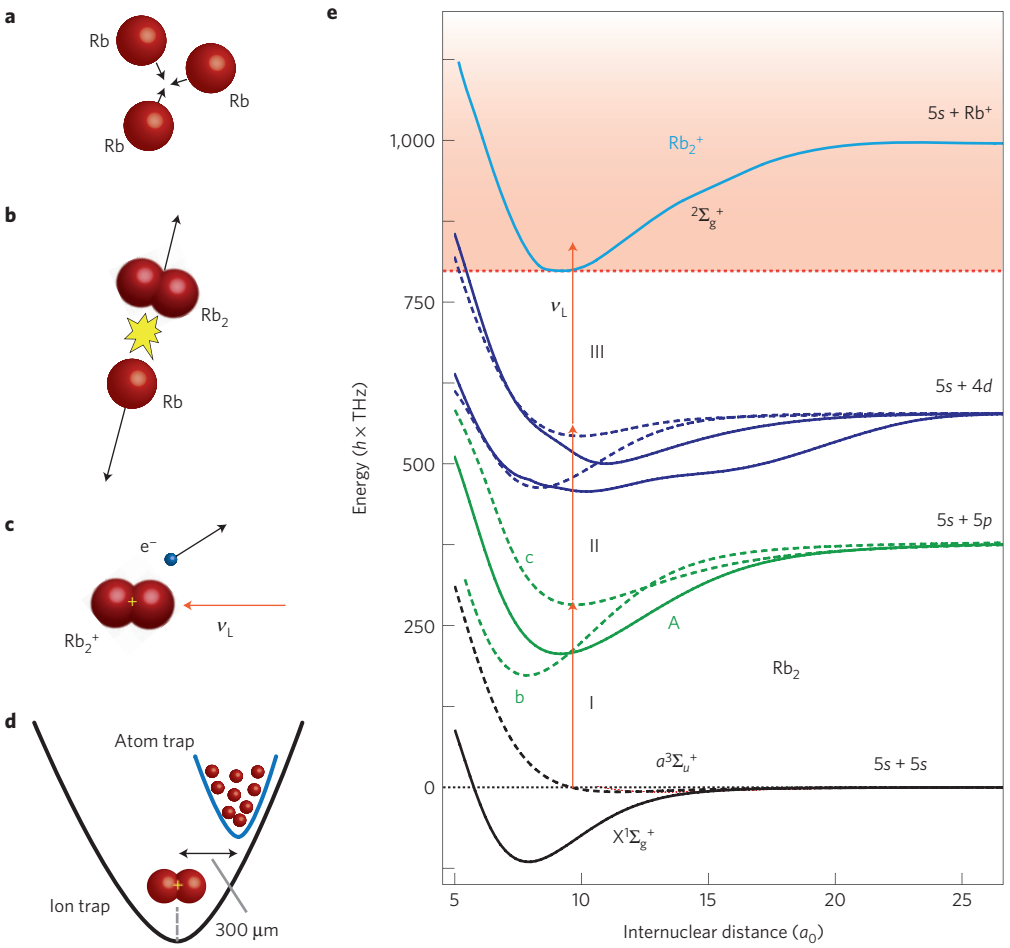

Figure 1 | Illustration of recombination and ionization in the atom–ion trap. a,**b**, A three-body collision in the ultracold gas of ^{87}Rb atoms (**a**) leads to a recombination event in which a Rb_2 molecule is formed with high kinetic energy (**b**). **c**, While the atom is lost from the trap, the molecule can be photoionized in a REMPI process and trapped in the Paul trap. **d**, The relative positions of the atom and ion trap centres are shifted by about 300 μm to avoid atom–ion collisions. **e**, Potential energy curves of the Rb_2 and Rb_2^+ molecule adapted from refs 18,35. The curves *A*, *b*, *c* are $A^1\Sigma_u^+$, $b^3\Pi_u$, $c^3\Sigma_u^+$. The internuclear distance is given in units of Bohr radii a_0. A REMPI path with three photons is shown. It can create Rb_2^+ ions in vibrational states up to $v \approx 17$.

k_B is the Boltzmann constant). The molecule, however, can be state-selectively ionized in a REMPI process driven by the dipole trap laser. All of these molecular ions remain trapped in the deep Paul trap and are detected with single-particle sensitivity (Methods). In each experimental run, we hold the atomic sample for a time $\tau \approx 10$ s. After this time we measure the number of produced ions in the trap from which we derive (after averaging over tens of runs) the ion production rate Γ_{ion} normalized to a cloud atom number of 10^6 atoms.

As a consistency check of our assumption that Rb_2 molecules are ionized in the REMPI process, we verify the production of Rb_2^+ molecules. For this, we perform ion mass spectrometry in the Paul trap (Methods). We detect primarily molecular Rb_2^+ ions, a good fraction of atomic Rb^+ ions but no Rb_3^+ ions. Our experiments show that Rb^+ ions are produced in light-assisted collisions of Rb_2^+ ions with Rb atoms on timescales below a few milliseconds. Details of this dissociation mechanism are under investigation and will be discussed elsewhere.

Two pathways for the production of our neutral Rb_2 molecules come immediately to mind. One pathway is far-off-resonant photoassociation of two colliding Rb atoms (here with a detuning of about 500 GHz × *h*). This pathway can be ruled out using several arguments, the background of which will be discussed in more depth later. For one, we observe molecules with a parity that is incompatible with photoassociation of totally spin-polarized ensembles. Furthermore, we observe a dependence of the ion production rate on light intensity that is too weak to explain photoassociation.

The second pathway is three-body recombination of Rb atoms. Indeed, by investigating the dependence of the ion production rate Γ_{ion} (which is normalized to a cloud atom number of 10^6 atoms) on atomic density, we find the expected quadratic dependence (Fig. 2). For this measurement the density was adjusted by varying the cloud atom number while keeping the light intensity of the dipole trap constant.

Next, we investigate the dependence of the ion production rate on the wavelength of the narrow-linewidth dipole trap laser (Methods). We scan the wavelength over a range of about 0.3 nm around 1,064.5 nm, corresponding to a frequency range of about 60 GHz. Typical frequency step sizes are 50 or 100 MHz. We obtain a rich spectrum of resonance lines that is shown in Fig. 3a. The quantity $\bar{\Gamma}_{ion}$ denotes the ion production rate normalized to the atom number of the cloud and to the square of the atomic peak density. We find strongly varying resonance strengths and at first sight fairly irregular frequency spacings. In the following we will argue that most resonance lines can be attributed to respective well-defined molecular levels (resolving vibrational, rotational and often even hyperfine structure) that have been populated in the recombination process. These levels are located in the triplet or singlet ground state, $a^3\Sigma_u^+$ and $X^1\Sigma_g^+$, respectively. The relatively

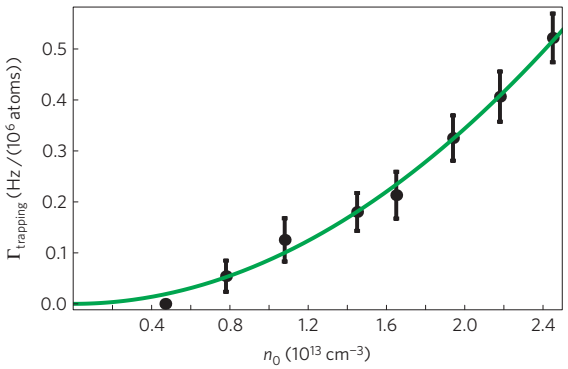

Figure 2 | Dependence of the ion production rate Γ_{ion} on atomic density. Γ_{ion} is normalized to a cloud atom number of 10^6 atoms. The data are well described by a quadratic fit (solid green line). They were taken at a constant dipole trap laser intensity $I_L = 36\,kW\,cm^{-2}$ and a laser frequency of $\nu_L = 281{,}630$ GHz. The error bars indicate statistical uncertainties and represent one standard deviation from the mean.

dense distribution of these lines reflects that a fairly broad range of states is populated. A direct assignment of the observed resonances is challenging, as it hinges on the precise knowledge of the level structure of all the relevant ground and excited states. In the following we will access and understand the data step by step.

One feature of the spectrum that stands out is the narrow linewidth of many lines. For example, Fig. 3b shows a resonance of which the substructures have typical half-widths $\Delta\nu_r \approx 50$ MHz. This allows us to roughly estimate the maximal binding energy of the molecules involved. As the velocity of the colliding ultracold atoms is extremely low, the kinetics of the recombination products is dominated by the released molecular binding energy E_b. Owing to energy and momentum conservation the molecules will be expelled from the reaction with a molecular velocity $v_{Rb2} = \sqrt{2E_b/(3m_{Rb2})}$, where m_{Rb2} is the molecular mass. The molecular resonance frequency ν_0 will then be Doppler-broadened with a half-width $\Delta\nu_D = \sqrt{3}\nu_0 v_{Rb2}/2c$. Here, c is the speed of light. By comparing $\Delta\nu_D$ to the observed values of $\Delta\nu_r$ we estimate a maximal binding energy of the order of $E_{b,max} \approx h \times 2.5$ THz. This simple analysis overestimates the value $E_{b,max}$ because it neglects the natural linewidth of the transition and possible saturation broadening. Still, it already strongly constrains the possibly populated molecular levels that are observed in our experiment.

Next, we investigate the dependence of the ion production rate on laser intensity I_L. In our experimental set-up, this measurement is rather involved because the laser driving the REMPI process also confines the atomic cloud. Thus, simply changing only the laser intensity would undesirably also change the density n_0 of the atoms. To prevent this from happening we keep n_0 constant ($n_0 \approx 5 \times 10^{13}$ cm^{-3}) by adjusting the atom number and temperature appropriately. Owing to these experimental complications we can vary I_L only roughly by a factor of 2 (Fig. 4a). We set the laser frequency to the value of $\nu_L = \nu_L^0 \equiv 281{,}610$ GHz, on the tail of a large resonance (Fig. 3). The atomic temperatures in this measurement range between 500 nK and 1.1 μK, well above the critical temperatures for Bose–Einstein condensation. The atomic densities can therefore be described using a Maxwell–Boltzmann

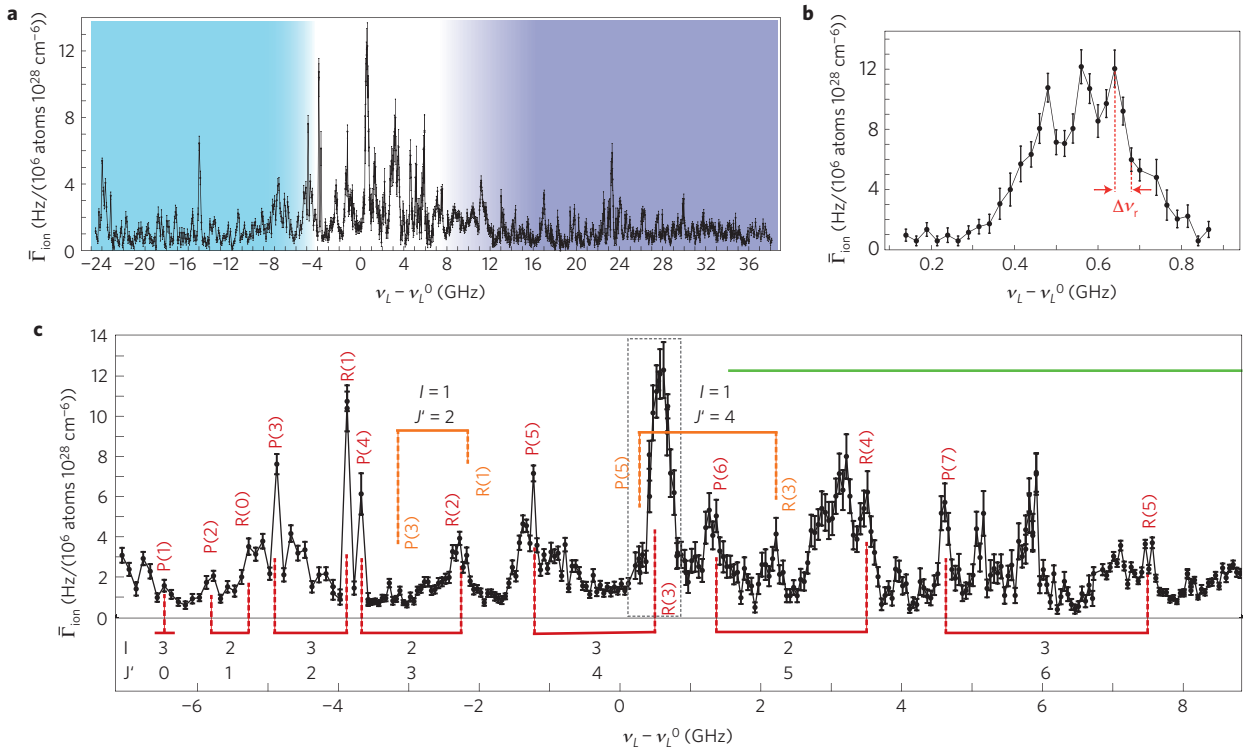

Figure 3 | REMPI spectrum. a, A scan of the dipole trap laser frequency ν_L over more than 60 GHz around an offset frequency $\nu_L^0 = 281.610$ THz shows a multitude of resonance lines. Each data point is the result of 30–60 repetitions of the experiment with ion detection on the single-particle level. The total spectrum was obtained over a time span of 2 months. Checks of the long-term consistency of resonance positions and strengths were performed. Spectral regions dominated by transitions to $c^3\Sigma_g^+$ are indicated by the shaded areas in dark and light blue (0_g^- and 1_g component, respectively). **b**, High-resolution scan of the strong resonance at $\nu_L - \nu_L^0 \approx 0.5$ GHz. **c**, Central spectral region with assigned P/R branches of the transition $X^1\Sigma_g^+(v = 115) \rightarrow A^1\Sigma_u^+(v' = 68)$. The corresponding quantum numbers I and J' are given. P(J) marks the transition $J \rightarrow J+1$; R(J) marks the transition $J \rightarrow J-1$. These lines can be grouped into pairs sharing the same J' of the excited state and I quantum number. The region where also transitions to $b^3\Pi_u$ appear is marked by a green horizontal bar. The error bars indicate statistical uncertainties and represent one standard deviation from the mean.

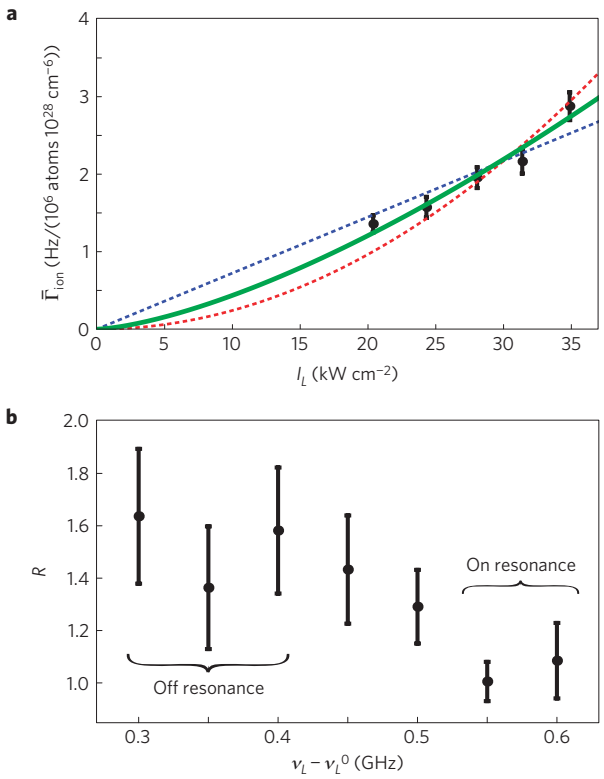

Figure 4 | Dependence of the ion production rate on the intensity of the dipole trap laser. a, Assuming a power-law dependence $\bar{\Gamma}_{ion} \propto I_L^{\alpha}$, the best fit to the data is achieved for $\alpha \approx 1.5$ (solid green line). Linear and quadratic fits are also given (blue and red dashed lines, respectively). **b**, Measurement of the intensity dependence using a chopped dipole trap. The ratio $R \approx 1$ on resonance indicates saturation of both transitions I and II. The error bars indicate statistical uncertainties and represent one standard deviation from the mean.

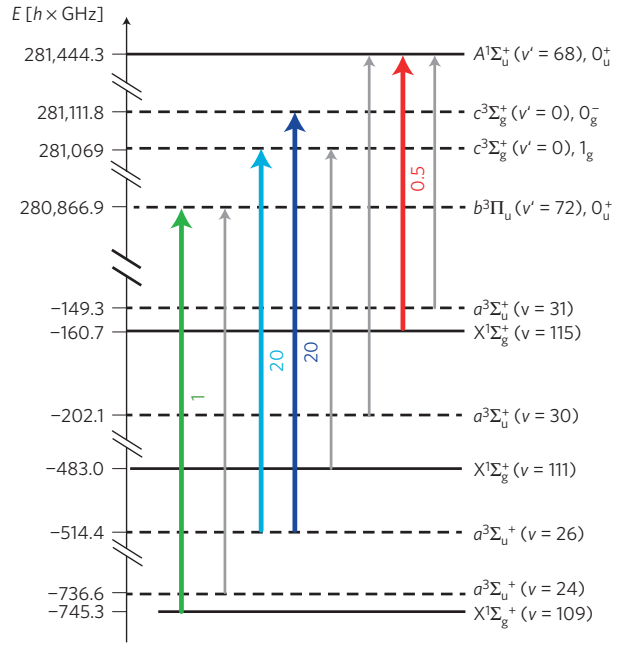

Figure 5 | Overview over relevant molecular levels and transitions. The vertical axis denotes the energy E_b of the energetically lowest levels of each vibrational manifold with respect to the 5s 5s asymptote. Coloured thick arrows represent molecular transitions relevant to the spectrum of Fig. 3. The expected relative strengths of these transitions are also given. Grey arrows mark transitions that occur in the relevant spectral region but are so weak that they can be neglected (for further spectroscopic details, see Methods). We identify three main molecular transitions for the initial step of the REMPI process. The blue arrows indicate molecules in the $v = 26$ vibrational level of the $a^3\Sigma_u^+$ potential that are excited to the $v' = 0$ level of the $c^3\Sigma_g^+$ potential. This level is split into a 1_g and a 0_g^- component. The red arrow is an excitation from $X^1\Sigma_g^+(v = 115)$ to $A^1\Sigma_u^+(v' = 68)$. The green arrow is an excitation from $X^1\Sigma_g^+(v = 109)$ to $b^3\Pi_u(v' = 72)$. This transition becomes possible through the strong spin–orbit coupling of the A and b states.

distribution. Assuming a simple power-law dependence of the form $\bar{\Gamma}_{ion} \propto I_L^{\alpha}$ we obtain the best fit using an exponent $\alpha = 1.5(1)$ (solid green line in Fig. 4a). This fit is between a linear and a quadratic intensity dependence (dashed red and blue lines, respectively). Thus, at least two of the three transitions composing the ionization process are partially saturated at the typical intensities used.

To better circumvent possible density variations of the atomic cloud induced by changes in laser intensity, we employ a further method that enables us to vary the intensity with negligible effects on the atomic sample. We achieve this by keeping the time-averaged intensity $\langle I_L \rangle$ constant and comparing the ion production rates within a continuous dipole trap and a chopped dipole trap in which the intensity is rapidly switched between 0 and $2I_L$. In both cases the trap is operated at an intensity $\langle I_L \rangle \approx 15\,\mathrm{kW\,cm^{-2}}$. In the chopped configuration the intensity is switched at a frequency of 100 kHz so that the atoms are exposed to the light for 5 µs followed by 5 µs without light. It should be noted that molecules formed in the dark period with sufficiently high kinetic energies may leave the central trapping region before the laser light is switched back on. They are then lost for our REMPI detection. Taking into account the molecular velocity and the transverse extensions of the laser beams we can estimate that this potential loss mechanism leads to errors of less than 30%, even at the highest binding energies relevant to this work ($E_b \approx h \times 750\,\mathrm{GHz}$, see below). We did not observe evidence of such losses experimentally. Investigations were made by changing the chopping frequency. We define R as the ratio of the ion production rates in the chopped and the continuous trap configuration. Figure 4b shows the results of these measurements for various laser frequencies ν_L. We find a value $R \approx 1.5$ for off-resonant frequency settings $\nu_L - \nu_L^0 < 0.4\,\mathrm{GHz}$, in good agreement with the result presented in Fig. 4a. When scanning the laser onto resonance at $\nu_L - \nu_L^0 \approx 0.45\,\mathrm{GHz}$ (Fig. 3b) we obtain $R \approx 1$. This result indicates a linear intensity dependence of the REMPI process in the resonant case, which is explained by the saturation of two of the three molecular transitions involved. It is known that transitions into the ionization continuum (photon III, Fig. 1e) will not saturate under the present experimental conditions. This means that the excitation pathway through photon I and II must be saturated and therefore both are close to resonance.

However, given the wavelength range of about 1,064.5 ± 0.15 nm, an inspection of the level structure shows that photon I can only resonantly drive three different transitions that connect vibrational levels in states X and a to vibrational levels in states A, b and c (Fig. 1e). Spectroscopic details for these transitions and the corresponding vibrational levels are given in the Methods and in Fig. 5. From recent spectroscopic studies[25–27] and further measurements in our laboratory the level structure of all relevant levels of the X, a, A, b, and c states is well known. The absolute precision of most of the level energies is far better than 1 GHz for low rotational quantum numbers J.

In the experimental data (Fig. 3a) the central region from $\nu_L - \nu_L^0 = -6$ to 7 GHz is marked by several prominent resonances that are significantly stronger than those observed throughout the rest of the spectrum. These resonance peaks can be assigned

to transitions from the X ground state to A and b states. The prominence of these singlet transitions is explained by the near degeneracy of levels due to small hyperfine splittings. Indeed, by analysing these strong resonances with regard to line splittings and intensities it was possible to consistently assign rotational ladders for total nuclear spin quantum numbers $I = 1$, 2, 3 for the transition $X(v = 115) \rightarrow A(v' = 68)$. The starting point of the rotational ladder for $I = 2$ was fixed by spectroscopic measurements in our laboratory. At frequencies $\nu_L - \nu_L^0 \gtrsim 2$ GHz additional strong lines appear that we attribute to the $X(v = 109) \rightarrow b(v' = 72)$ transition. The fact that we observe X state molecules with $I = 1$, 2, 3 is interesting because for $I = 1$, 3 the total parity of the molecule is negative, whereas for $I = 0$, 2 it is positive. However, a two-body collision state of our spin-polarized Rb atoms necessarily has positive total parity due to symmetry arguments and a photoassociation pathway would lead to ground-state levels with positive parity. The observed production of molecules with negative total parity must then be a three-body collision effect.

We now consider the role of secondary atom–molecule collisions that would change the product distribution owing to molecular relaxation. Two aspects are of importance: depopulation of detected molecular levels, and population of detected molecular levels through relaxation from more weakly bound states. In our experiments reported here we detect molecules that are formed in states with binding energies of the order of hundreds of GHz $\times h$. These molecules leave the reaction with kinetic energies of several $K \times k_B$. At these energies the rate coefficients for depopulating atom–molecule collisions are small (see for example ref. 15) and the collision probability before the molecule is either ionized or has left the trap is below 1%.

For the population processes, we can estimate an upper bound for rate coefficients by assuming recombination to occur only into the most weakly bound state with a binding energy of 24 MHz $\times h$. In this case subsequent atom–molecule collision rates will be roughly comparable to those expected in the ultracold limit. At typical rate coefficients of 10^{-10} cm^3 s^{-1} (refs 28–31) and the atomic densities $n_0 \sim 1 \times 10^{13}$ cm^{-3} used in the measurement shown in Fig. 2, the collision probability before the molecule leaves the atom cloud is around 5%. This small probability grows linearly with density so that the density dependence of the ion production rate should show a significant cubic contribution if secondary collisions were involved (as expected for this effective four-body process). This is inconsistent with the data and thus indicates that the population that we detect is not significantly altered by secondary collisions.

We can roughly estimate the range of molecular rotation J of the populated levels in the ground state. The strong, isolated lines that we have assigned to the $X(v = 115) \rightarrow A(v' = 68)$ transition are all contained within a relatively small spectral region ($|\nu_L - \nu_L^0| < 6$ GHz) and are explained by rotational quantum numbers $J \leq 7$. Population of higher rotational quantum numbers would result in a continuation of the strong resonance lines stretching to transition frequencies beyond $\nu_L - \nu_L^0 = 10$ GHz, which we do not observe. Similarly, if only rotational quantum numbers $J \leq 5$ were populated, a spectrum would result that does not have enough lines to explain the data. Thus, we can roughly set the limits on the molecular rotation to $J \leq 7$, a value that is also consistent with our observations of the spread of the transitions $X \rightarrow b$ and $a \rightarrow c$ (Fig. 5). Finding quantum numbers as high as $J = 7$ is remarkable because the three-body collisions at microkelvin temperatures clearly take place in an s-wave regime, that is, at vanishing rotational angular momentum. Hence, one could expect to produce X state molecules dominantly at $J = 0$, which, however, we do not observe.

Despite the limited spectral range covered by our measurements, we can already estimate the number of molecular vibrational levels populated in the recombination events. From the three states $X(v = 109)$, $a(v = 26)$ and $X(v = 115)$ that we can observe within our wavelength range, all deliver comparable signals in the spectrum of Fig. 3. This suggests that at least all vibrational states more weakly bound than $X(v = 109)$ should be populated, a total of 38 vibrational levels (counting both singlet and triplet states). This is a significant fraction of the 169 existing levels of the X and a states, although restricted to a comparatively small range of binding energies.

In conclusion, our work represents a first experimental step towards a detailed understanding on how the reaction channels in three-body recombination are populated. A full understanding will clearly require further experimental and theoretical efforts. On the experimental side the scanning range has to be increased and it could be advantageous to switch to a two-colour REMPI scheme in the future. Such studies may finally pave the way to a comprehensive understanding of three-body recombination, which includes the details of the final products.

Reaching beyond the scope of three-body recombination, the great sensitivity of our detection scheme has enabled us to state-selectively probe single molecules that are produced at rates of only a few hertz. We thereby demonstrate a new scheme for precision molecular spectroscopy in extremely dilute ensembles.

Methods

Dipole trap and REMPI configuration. The crossed dipole trap is composed of a horizontal and a vertical beam focused to beam waists of ~90 μm and ~150 μm, respectively. It is positioned onto the nodal line of the radiofrequency field of the linear Paul trap with micrometre precision. The two trap centres are separated by about 300 μm along the axis of the Paul trap (Fig. 1d). In a typical configuration, the trap frequencies of the dipole trap are (175, 230, 80) Hz resulting in atom cloud radii of about (6, 7, 16) μm. The short-term frequency stability of the dipole trap laser source is of the order of 1 kHz and it is stabilized against thermal drifts to achieve long-term stability of a few megahertz. The two beams of the dipole trap are mutually detuned by 160 MHz to avoid interference effects in the optical trap. Consequently, two frequencies are in principle available to drive the REMPI process. However, the intensity of the horizontal beam is 4 times larger than the one of the vertical beam and we have not directly observed a corresponding doubling of lines. Further details on the atom–ion apparatus are given in ref. 32.

Paul trap configuration. The linear Paul trap is driven at a radiofrequency of 4.17 MHz and an amplitude of about 500 V resulting in radial confinement with trap frequencies of $(\omega_{x,\mathrm{Ba}}, \omega_{y,\mathrm{Ba}}) = 2\pi \times (220, 230)$ kHz for a $^{138}Ba^+$ ion. Axial confinement is achieved by applying static voltages to two endcap electrodes yielding $\omega_{z,\mathrm{Ba}} = 2\pi \times 40.2$ kHz. The trap frequencies for dark Rb_2^+ and Rb^+ ions produced in the REMPI processes are $(m_{\mathrm{Ba}}/m_{\mathrm{dark}} \times \omega_{x,\mathrm{Ba}}, m_{\mathrm{Ba}}/m_{\mathrm{dark}} \times \omega_{y,\mathrm{Ba}}, \sqrt{m_{\mathrm{Ba}}/m_{\mathrm{dark}}} \times \omega_{z,\mathrm{Ba}})$, where m_{Ba} and m_{dark} denote the mass of the Ba^+ ion and the dark ion, respectively. The depth of the Paul trap depends on the ionic mass and exceeds 2 eV for all ionic species relevant to this work.

Ion detection methods. We employ two methods to detect Rb_2^+ and Rb^+ ions, both of which are not amenable to fluorescence detection. In the first of these methods we use a single trapped and laser-cooled $^{138}Ba^+$ ion as a probe. By recording its position and trapping frequencies in small ion strings with up to 4 ions we detect both the number and the masses of the ions following each REMPI process (see also ref. 33). The second method is based on measuring the number of ions in the Paul trap by immersing them into an atom cloud and recording the ion-induced atom loss after a hold time of 2 s (see also ref. 34). During this detection scheme, we take care to suppress further generation of ions by working with small and dilute atomic clouds and by detuning the REMPI laser from resonance. Both methods are background-free in the sense that no ions are captured on timescales of days in the absence of the atom cloud. Further information on both detection methods is given in the Supplementary Information.

Spectroscopic details. Spin–orbit and effective spin–spin coupling in the A, b, and c states lead to Hund's case c coupling where the relevant levels of states A and b have 0_u^+ symmetry whereas the levels of state $c^3\Sigma_g^+$ are grouped into 0_g^- and 1_g components. The level structure of the 0_u^+ states is quite simple as it is dominated by rotational splittings. Typical rotational constants for the electronically excited states are of the order of 400 MHz; for the weakly bound X and a states they are around 100–150 MHz.

Figure 5 shows the relevant optical transitions between the X, a states and the A, b, c states in our experiment. For the given expected relative strengths of these transitions, we consider only Franck–Condon factors and the mixing of singlet and triplet states, and electronic transition moments are ignored. The coloured arrows

correspond to transitions with large enough Franck–Condon factors (typically 10^{-2}–10^{-3}) so that at laser powers of $\approx 10^4$ W cm^{-2} resonant transitions can be well saturated. Transitions marked with grey arrows can be neglected owing to weak transition strengths, being forbidden in first order by dipole selection rules.

Received 23 January 2013; accepted 14 May 2013; published online 23 June 2013

References

1. Hess, H. F. *et al.* Observation of three-body recombination in spin-polarized hydrogen. *Phys. Rev. Lett.* **51,** 483–486 (1983).
2. Burt, E. A. *et al.* Coherence, correlations, and collisions: What one learns about Bose–Einstein condensates from their decay. *Phys. Rev. Lett.* **79,** 337–340 (1997).
3. Söding, J. *et al.* Three-body decay of a rubidium Bose–Einstein condensate. *Appl. Phys. B* **69,** 257–261 (1999).
4. Esry, B. D., Greene, C. H. & Burke, J. P. Recombination of three atoms in the ultracold limit. *Phys. Rev. Lett.* **83,** 1751–1754 (1999).
5. Suno, H. & Esry, B. D. Three-body recombination in cold helium–helium-alkali-metal-atom collisions. *Phys. Rev. A* **80,** 062702 (2009).
6. Wang, Y., D'Incao, J. P. & Esry, B. D. Cold three-body collisions in hydrogen–hydrogen-alkali-metal atomic systems. *Phys. Rev. A* **83,** 032703 (2011).
7. Guevara, N. L., Wang, Y. & Esry, B. D. New class of three-body states. *Phys. Rev. Lett.* **108,** 213202 (2012).
8. Fedichev, P. O., Reynolds, M. W. & Shlyapnikov, G. V. Three-body recombination of ultracold atoms to a weakly bound *s* level. *Phys. Rev. Lett.* **77,** 2921–2924 (1996).
9. Bedaque, P. F., Braaten, E. & Hammer, H-W. Three-body recombination in Bose gases with large scattering length. *Phys. Rev. Lett.* **85,** 908–911 (2000).
10. Efimov, V. Energy levels arising from resonant two-body forces in a three-body system. *Phys. Lett. B* **33,** 563–564 (1970).
11. Braaten, E. & Hammer, H-W. Three-body recombination into deep bound states in a Bose gas with large scattering length. *Phys. Rev. Lett.* **87,** 160407 (2001).
12. Kraemer, T. *et al.* Evidence for Efimov quantum states in an ultracold gas of caesium atoms. *Nature* **440,** 315–318 (2006).
13. Weber, T., Herbig, J., Mark, M., Nägerl, H-C. & Grimm, R. Three-body recombination at large scattering lengths in an ultracold atomic gas. *Phys. Rev. Lett.* **91,** 123201 (2003).
14. Jochim, S. *et al.* Pure gas of optically trapped molecules created from Fermionic atoms. *Phys. Rev. Lett.* **91,** 240402 (2003).
15. Simoni, A. & Launay, J-M. Ultracold atom-molecule collisions with hyperfine coupling. *Laser Phys.* **16,** 707–712 (2006).
16. Bates, D. R., Kingston, A. E. & McWhirter, R. W. P. Recombination between electrons and atomic ions. I. Optically thin plasmas. *Proc. R. Soc. Lond. Ser A.* **267,** 297–312 (1962).
17. Flower, D. R. & Harris, G. J. Three-body recombination of hydrogen during primordial star formation. *Mon. Not. R. Astronom. Soc.* **377,** 705–710 (2007).
18. Lozeille, J. *et al.* Detection by two-photon ionization and magnetic trapping of cold Rb_2 triplet state molecules. *Eur. Phys. J. D* **39,** 261–269 (2006).
19. Fioretti, A. *et al.* Formation of cold Cs_2 molecules through photoassociation. *Phys. Rev. Lett.* **80,** 4402–4405 (1998).
20. Gabbanini, C., Fioretti, A., Lucchesini, A., Gozzini, S. & Mazzoni, M. Cold rubidium molecules formed in a magneto-optical trap. *Phys. Rev. Lett.* **84,** 2814–2817 (2000).
21. Huang, Y. *et al.* Formation, detection and spectroscopy of ultracold Rb_2 in the ground $X^1\Sigma_g^+$ state. *J. Phys. B* **39,** S857–S869 (2006).
22. Salzmann, W. *et al.* Coherent transients in the femtosecond photoassociation of ultracold molecules. *Phys. Rev. Lett.* **100,** 233003 (2008).
23. Sullivan, S. T. *et al.* Trapping molecular ions formed via photo-associative ionization of ultracold atoms. *Phys. Chem. Chem. Phys.* **13,** 18859–18863 (2011).
24. Mudrich, M. *et al.* Spectroscopy of triplet states of Rb_2 by femtosecond pump–probe photoionization of doped helium nanodroplets. *Phys. Rev. A* **80,** 042512 (2009).
25. Strauss, C. *et al.* Hyperfine, rotational, and vibrational structure of the $a^3\Sigma_u^+$ state of $^{87}Rb_2$. *Phys. Rev. A* **82,** 052514 (2010).
26. Takekoshi, T. *et al.* Hyperfine, rotational, and Zeeman structure of the lowest vibrational levels of the $^{87}Rb_2$ (1) $^3\Sigma_g^+$ state. *Phys. Rev. A* **83,** 062504 (2011).
27. Drozdova, A. *Study of Spin-Orbit Coupled Electronic States of* Rb_2, *NaCs and NaK Molecules. Laser Spectroscopy and Accurate Coupled-channel Deperturbation Analysis* PhD thesis, Univ. de Lyon and Lomonosov State Univ. (2012).
28. Mukaiyama, T., Abo-Shaeer, J. R., Xu, K., Chin, J. K. & Ketterle, W. Dissociation and decay of ultracold sodium molecules. *Phys. Rev. Lett.* **92,** 180402 (2004).
29. Staanum, P., Kraft, S. D., Lange, J., Wester, R. & Weidemüller, M. Experimental investigation of ultracold atom-molecule collisions. *Phys. Rev. Lett.* **96,** 023201 (2006).
30. Zahzam, N., Vogt, T., Mudrich, M., Comparat, D. & Pillet, P. Atom-molecule collisions in an optically trapped gas. *Phys. Rev. Lett.* **96,** 023202 (2006).
31. Quéméner, G., Launay, J-M. & Honvault, P. Ultracold collisions between Li atoms and Li_2 diatoms in high vibrational states. *Phys. Rev. A* **75,** 050701 (2007).
32. Schmid, S., Härter, A., Frisch, A., Hoinka, S. & Hecker Denschlag, J. An apparatus for immersing trapped ions into an ultracold gas of neutral atoms. *Rev. Sci. Instrum.* **83,** 053108 (2012).
33. Schmid, S., Härter, A. & Hecker Denschlag, J. Dynamics of a cold trapped ion in a Bose–Einstein condensate. *Phys. Rev. Lett.* **105,** 133202 (2010).
34. Härter, A. *et al.* Single ion as a three-body reaction center in an ultracold atomic gas. *Phys. Rev. Lett.* **109,** 123201 (2012).
35. Aymar, M., Azizi, S. & Dulieu, O. Model-potential calculations for ground and excited Σ states of Rb_2^+, Cs_2^+ and $RbCs^+$ ions. *J. Phys. B* **36,** 4799–4812 (2003).

Acknowledgements

The authors would like to thank S. Schmid and A. Brunner for support during early stages of the experiment and O. Dulieu, B. Esry, J. d'Incao, W. Stwalley, U. Heinzmann, J. Hutson, P. Soldan, T. Bergeman and A. Drozdova for valuable information and fruitful discussions. This work was supported by the German Research Foundation DFG within the SFB/TRR21.

Author contributions

A.H. and A.K. performed the experiments in the atom–ion trap set-up; M.D. and B.D. performed spectroscopic measurements on Rb_2 molecules; A.H., A.K., E.T. and J.H.D. analysed data; A.H., E.T. and J.H.D. wrote the paper.

Additional information

Supplementary information is available in the online version of the paper. Reprints and permissions information is available online at www.nature.com/reprints. Correspondence and requests for materials should be addressed to J.H.D.

Competing financial interests

The authors declare no competing financial interests.